Desalination and Water Treatment
www.deswater.com
doi: 10.5004/dwt.2022.29064

279 (2022) 29–35
December

Humic acid removal from water using *Moringa* protein functionalized biochar husk

Abdelhek Belbali*, Abderrezak Benghalem, Khadidja Gouttal, Safia Taleb, Fatima Zohra Ziri

Laboratory of Materials and Catalysis (LMC), Department of Chemistry, Faculty of Exacte Sciences, University of Djillali Liabes, Sidi Bel Abbes, Algeria, Tel. +213 671904476; email: belbaliabdelhak@gmail.com (A. Belbali), Tel. +213 773246760; email: benghalem_has@yahoo.fr (A. Benghalem), Tel. +213 791061585; email: gouttalkhadidja@gmail.com (K. Gouttal), Tel. +213 560809933; email: safiatal@yahoo.fr (S. Taleb), Tel. +213 541999125; email: ziri.fatimazohra@gmail.com (F.Z. Ziri)

Received 1 July 2022; Accepted 8 October 2022

ABSTRACT

Biochar obtained from *Moringa* seeds husks was functionalized with protein extracted from *Moringa* kernels powder resulting in a composite biochar (BC-MOP). The functionalization of its surface was characterized by FTIR spectroscopy, which showed the appearance of peaks indicative of protein functions (amines and ketones), confirming the consolidation of the surface. This composite was tested in humic acid (HA) removal from an aqueous solution, and its adsorption capacity was evaluated by comparison with that of biochar (BC). Removal rates favored the composite 81.4 mg g^{-1} for BC-MOP and 41 mg g^{-1} for BC when the temperature was 25°C which demonstrated the impact of functionalization. The operating parameters pH, contact time, and dose of adsorbent were optimized, and it was found that solution pH played a crucial role in the adsorption process. The adsorption isotherms of the HA fit the Langmuir model better than the Freundlich model, and the adsorption kinetics followed the pseudo-second-order model. The adsorption was chemisorption in nature. The degradation of HA into units of low molecular weight substances was proved by FTIR spectrum and UV absorption after adsorption of HA. This study contributed to the development of new composite biochars with high adsorbent capacity toward organic pollutants.

Keywords: Biochar; *Moringa* protein; Humic acid; Adsorption; Functionalized biochar

1. Introduction

In surface and groundwater, humic acid (HA) is a key component of humic compounds resulting from biomolecules' microbial breakdown [1,2]. The water supply sector has struggled with HA for a very long time. HA in drinking water can cause issues with its appearance, flavor, and odor, as well as biological instability in the distribution system [2]. Additionally, numerous pollutants can be bound by HA, such as dangerous heavy metals and man-made organic substances like pesticides, and transported through water treatment and distribution systems [3]. More significantly, HA can combine with chlorine during water treatment to create highly carcinogenic disinfection by-products, including trihalomethanes [1–3].

Many techniques, including coagulation/flocculation, membrane separation, advanced oxidation, ion exchange, and adsorption, have been developed to remove HA during water treatment [4]. Adsorption has been regarded as one of them due to its high efficiency, straightforward operation, and simple design [5]. Several adsorbents have been used for the adsorption of HA in an aqueous solution,

* Corresponding author.

Presented at the First International Congress of Energy and Industrial Process Engineering (ICEIPE'22) 23–25 May 2022, Algiers, Algeria

including activated carbon, graphene, iron oxides, polymers, biomass-based biochar, clay minerals, and oxides and nanocomposites.

Among these sorbents, biochar has been used successfully to remove various contaminants from soil and water, including heavy metals, organic pollutants, and microbiological contaminants [6,7]. It has been demonstrated that biochar is a porous carbon-based material produced when carbon-rich material was heated to a high temperature and then burned at a low oxygen level [7]. The advantages of using biochar as an adsorbent with superior adsorption capabilities for removing organic pollutants and heavy metals include particular surface areas, pore architectures, furthermore the degree of surface functional groups that contain oxygen (O) [6,8]. However, a lot of effort has recently been focused on synthesizing new functionalized biochars with changed surface characteristics to improve their adsorption capabilities, and possible potential uses to rehabilitate the ecosystem [9,7].

It was discovered that the aqueous extract of MO seed kernels contained positively charged peptides with low molecular masse, which can be used as a coagulant for water and wastewater treatment. Furthermore, the coagulant protein from MO was also shown to be a dimeric 13 kDa protein with components of 6.5 kDa containing coagulating activity [10]. Adsorption and charge neutralization is thought to form the foundation of the MO protein's coagulation process [10,11].

In this study, the surface of biochar (BC) was modified with *Moringa* protein (MOP) to prepare *Moringa* protein-functionalized biochar (BC-MOP) and utilized for the adsorption of HA from an aqueous solution. The synthesized BC-MOP was characterized by Fourier transform infrared spectroscopy (FTIR), X-ray diffraction (XRD), and scanning electron microscopy (SEM). The HA adsorption process on BC and BC-MOP was investigated as a function of pH, adsorbents mass, contact time, and adsorbate concentration. The FTIR and UV spectrophotometry of HA solution before and after treatment were studied.

2. Materials and methods

2.1. Adsorbent preparation

2.1.1. Biochar production

The husks of *Moringa* seeds were harvested between September and October 2020 from trees grown to Adrar, Algeria. *Moringa* husks were washed three times with distilled water to eliminate any contaminants of the surface then dried overnight at 80°C. Then the husks were ground to obtain powder using a grinder. Ceramic crucibles were filled with husk powder, covered with a fitted lid, and pyrolyzed under oxygen-limited conditions in a muffle furnace (Nabertherm, Germany) at 450°C for 1 h. The biochar was immediately cooled at room temperature to activate the surface pores.

2.1.2. Moringa protein -functionalized biochar preparation

Moringa protein extraction, as well as the characterizations, were reported in detail previously [12]. *Moringa* protein (MOP) suspension was made by 1 g of MOP and 1 L of distilled water. MOP-functionalized biochar (BC-MOP) was prepared by dispersion of biochar particles in MOP suspension with a rapport of 2:1 (g/g) at a temperature of 30°C. The mixture was agitated for 3 h using a rotary shaker.

2.1. Adsorption experiments

Batch adsorption experiments of HA on BC and BC-MOP were carried out in a 250 mL Erlenmeyer with 50 mL of HA solution. The effect of operating parameters (pH 3–10, adsorbents dose, and contact time) was studied. pH was adjusted by adding 0.1 M of HCl or 0.1 M of NaOH. The residual concentration of HA in the supernatant was determined at 254 nm with a UV/VIS spectrophotometer (PERKIN ELMER). The effect of HA concentration on the experiments was recorded by varying the concentrations of HA between (0–300 mg/L). The HA adsorption capacity was calculated according to the following equation:

$$q_{\text{ads}} = \frac{C_0 - C_e}{m} V \tag{1}$$

where q_{ads}: the amount of HA adsorbent (mg/g); C_0: initial concentration of HA (mg/L); C_e: equilibrium concentration mg/L; V: volume (L); m: mass of adsorbent (g).

2.2. Kinetic and isotherm adsorption models

The kinetic data was analyzed using pseudo-first-order (PFO) and pseudo-second-order (PSO). The nonlinear PFO equation is as follows:

$$q_t = q_e\left[1 - \exp\left(-K_1 t\right)\right] \tag{2}$$

The linearized form is as below [13]:

$$\ln\left(q_e - q_t\right) = \ln q_e - K_1 t \tag{3}$$

The nonlinear PSO equation is as follows:

$$q_t = \frac{K_2 q_e^2 t}{1 + q_e K_2 t} \tag{4}$$

The linearized form is as below [13]:

$$\frac{t}{q_t} = \frac{1}{k_2 q_e^2} + \frac{t}{q_e} \tag{5}$$

where q_t represent the quantity of adsorbate at any given time t, q_e is the amount of adsorbate at equilibrium time (mg g^{-1}), and k_1 (min^{-1}) and k_2 (g mg^{-1} min^{-1}) are the pseudo-first-order and pseudo-second-order equilibrium rate constants, respectively.

Two isothermal models; Langmuir [Eq. (6)] and Freundlich [Eq. (7)] were used to fit experimental data.

The nonlinear equations are as follows:

$$q_e = \frac{q_m K_L C_e}{1 + K_L C_e} \tag{6}$$

$$q_e = K_F C_e^{1/n} \tag{7}$$

The linearized forms of these models were as follows [14]:

$$\frac{C_e}{q_e} = \frac{1}{q_m K_L} + C_e \frac{1}{q_m} \tag{8}$$

$$\log q_e = \log K_F + \frac{1}{n} Log C_e \tag{9}$$

where C_e (mg L^{-1}) denote the HA solution equilibrium concentration, q_e and q_m (mg g^{-1}) denotes the quantity adsorbed and maximum adsorption capacity, respectively, and k_L denotes the Langmuir constant (L mg^{-1}). The Freundlich affinity coefficient is K_F (mg/g)(L/mg)$^{1/n}$, and n is a measure of adsorption linearity.

3. Results and discussion

3.1. Characterization of adsorbents

3.1.1. FTIR analysis

The FTIR of BC and BC-MOP spectra are shown in Fig. 1. The peak at 1,592 cm^{-1} in the FTIR spectrum of BC represents C=O stretching mode coupled with NH_2 (amide group) [15]. The transmittance peak at 1373 cm^{-1} was attributed to C–H bending vibration [16]. The peak at 1,449 cm^{-1} was assigned to aromatic C=C stretching vibration. The C–O–C symmetric stretching typical of cellulose and hemicellulose was attributed to the peak detected at 1119 cm^{-1} [17]. All of the distinctive peaks in the FTIR spectrum of the BC-MOP were sharper than those in the BC spectrum, demonstrating that MOP modification of *Moringa* husks biochar can effectively increase the number of active functional groups on the BC surface. The peak appearing at 2,995 cm^{-1} was attributed to stretching vibrations of C–H groups indicating that the protein had been introduced onto the BC surface.

3.1.2. XRD analysis

Fig. 2 shows the XRD diffractograms of BC and BC-MOP. Broad diffraction peaks in the BC and BC-MOP at 2Θ = 25° correspond to the graphite (002) crystal face diffraction of amorphous carbon [18]. Other tiny peaks can be seen in the XRD pattern of BC, indicating a significant number of weakly crystalline phases such as calcite ($CaCO_3$) and fluorite (CaF_2). Meanwhile, the XRD pattern of BC-MOP is nearly identical to that of BC, showing that the addition of MOP during the synthesis process has no substantial impact on the product's crystal shape.

3.1.3. SEM analysis

The effect of protein addition on the structural morphology of BC was investigated using SEM characterization. Fig. 3 depicts an exemplary SEM image of BC-MOP. According to this image, BC-MOP has an irregular, solid coarse, and heterogeneous surface with many mesopores.

3.2. Effect of pH on adsorption process

The effect of pH on the HA removal was conducted in the pH 3–10 range. Fig. 4a demonstrates that for both BC and BC-MOP, the highest elimination was attained at pH 3 doses. As shown in Fig. 4b, the PZC of BC and BC-MOP are respectively 7.8 and 7.4; this indicates that for pH higher than PZC, the adsorbent surface charge is negative. The positive charge magnitude on the particle edges gradually grows when pH gradually drops below this level. The HA removal increases for pH levels below PZC because BC and BC-MOP surfaces carry a positive charge, and the anionic species (COO–, phenolic) prevailing at this pH; this will favor HA adsorption. As the pH rises, the

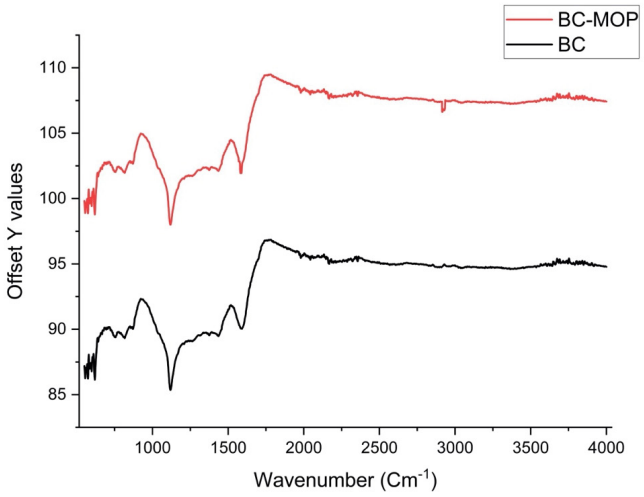

Fig. 1. FTIR spectra of BC and BC-MOP.

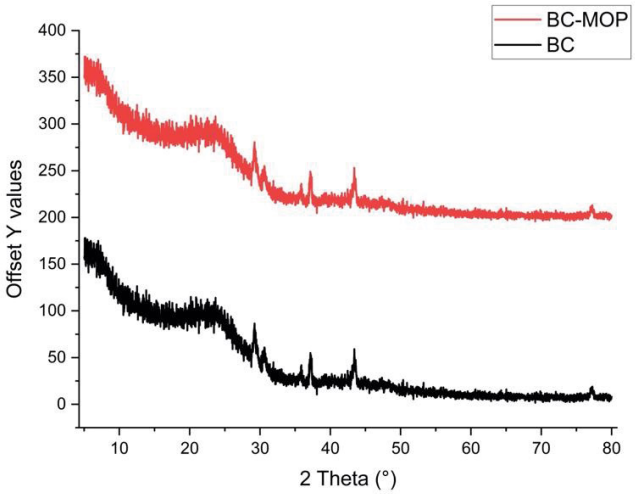

Fig. 2. X-ray diffractograms of BC and BC-MOP.

surface charge of BC and BC-MOP progressively decreases to zero, then turns negative for pH greater than PZC. In this instance, the reduction in the adsorption is a result of repulsion between the negative charge developed on the surface of adsorbents and the anionic species of HA.

3.3. Effect of adsorbents dosage

As shown in Fig. 5, the adsorption capacity of HA was found to increase with the increase of adsorbents dosages, this is due to the increase of adsorbents' active sites and the surface area of adsorbents. The maximum adsorption capacity was obtained with the dose of 1 g/L.

3.4. Effect of contact time

As shown in Fig. 6a, the adsorption kinetics of HA on BC and BC-MOP were evaluated by varying contact times between 0–150 min using a fixed initial concentration of HA (50 mg/L) and pH = 3. As seen the equilibrium time of HA adsorption on BC was faster than that for BC-MOP, the times were respectively 50 and 150 mn, however the adsorption rate of BC-MOP was much higher than BC. Fig. 6b shows that the adsorption kinetics are of second-order. From the results of Table 1 which were obtained from the linearized equation, the R^2 coefficients of PSO showed higher values compared to those of PFO. The R^2 coefficients of the PSO are 0.998 and 0.999, while the R^2 coefficients of the PFO are 0.669 and 0.97 for BC-MOP and BC respectively. Moreover the adsorption capacities calculated for PSO are much closer to experimental capacities, meaning that the chemisorption plays a significant part in the adsorption process [19].

3.5. Effect of initial HA concentration

For HA adsorption on BC and BC-MOP, isotherm plots show that adsorption rises as HA concentration rises,

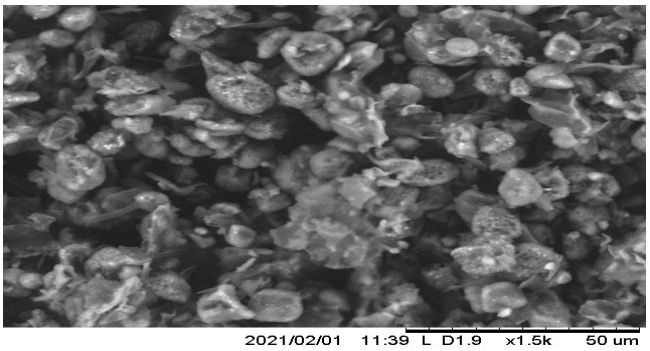

Fig. 3. SEM image of BC-MOP.

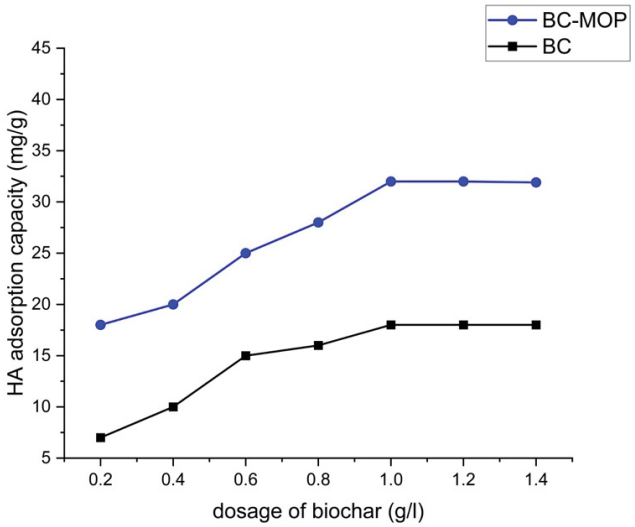

Fig. 5. Effect of adsorbents dosage on HA adsorption (pH = 3).

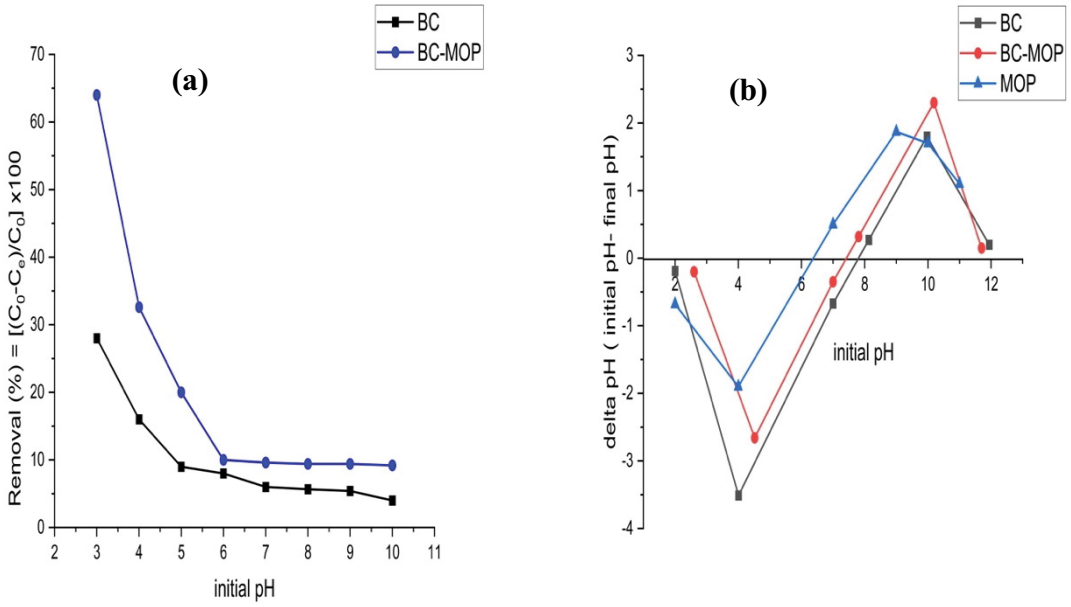

Fig. 4. (a) Effect of initial pH on HA adsorption and (b) PZC of BC, BC-MOP, and MOP.

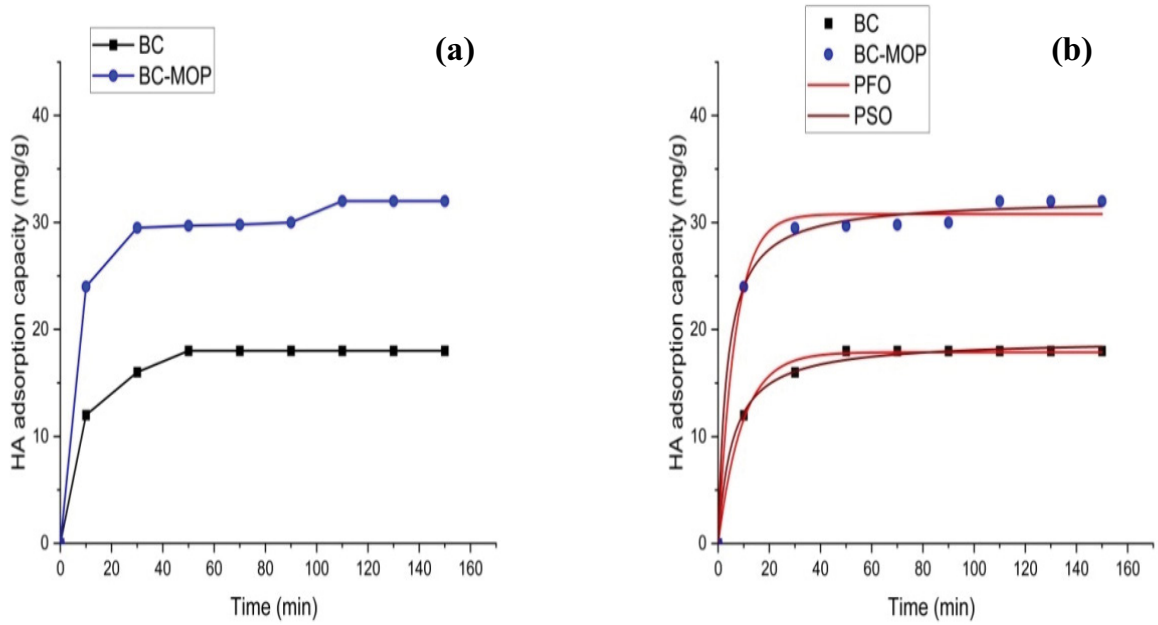

Fig. 6. (a) Effect of contact time and (b) fitted kinetic models with 1 g/L dosage of adsorbents at pH 3 and 25°C.

Table 1
Kinetic parameters for HA removal

Kinetic model	Adsorbent	Parameters		
PFO		q_e (mg/g)	K_1 (min^{-1})	R^2
	BC-MOP	12.66	0.025	0.669
	BC	15.33	0.073	0.970
PSO		q_e (mg/g)	K_2 (min^{-1})	R^2
	BC-MOP	32.91	6.28 10^{-3}	0.998
	BC	18.58	1.46 10^{-2}	0.999

demonstrating that HA dosage functions as an adsorption-inducing force (Fig. 7). The nonlinear Langmuir and Freundlich isotherms models were fitted (Fig. 7b), and their characteristics parameters were obtained from the linearized equations (Table 2). With a comparison of correlation coefficient R^2, the Langmuir isotherm model shows the best fit of HA adsorption on BC and BC-MOP. Notably, the K_L value of BC-MOP was higher than that of BC, showing that the surface of BC had formed additional functional groups, which led to the increased adsorption energy. The maximum adsorption capacities of 87.10 and 45.06 mg/g were obtained through the Langmuir model for BC-MOP and BC, respectively, are more consistent with the experimental

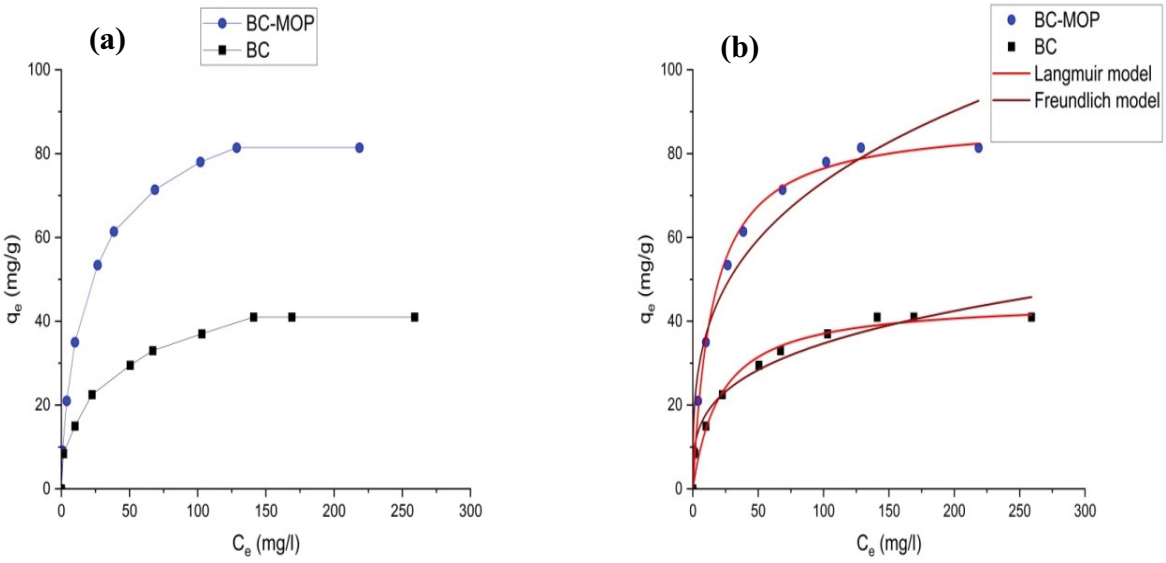

Fig. 7. (a) Effect of HA acid concentration and (b) fitted isotherms models with 1 g/L dosage of adsorbents at pH = 3 and 25°C.

Table 2
Langmuir and Freundlich parameters on the adsorption of HA

Model	Adsorbent	Isotherm parameters		
Langmuir		q_m (mg/g)	K_L (L/mg)	R^2
	BC-MOP	87.10	0.076	0.997
	BC	45.06	0.044	0.998
Freundlich		n	K_F (mg/g)(L/mg)$^{1/n}$	R^2
	BC-MOP	2.45	11.80	0.867
	BC	2.36	4.94	0.898

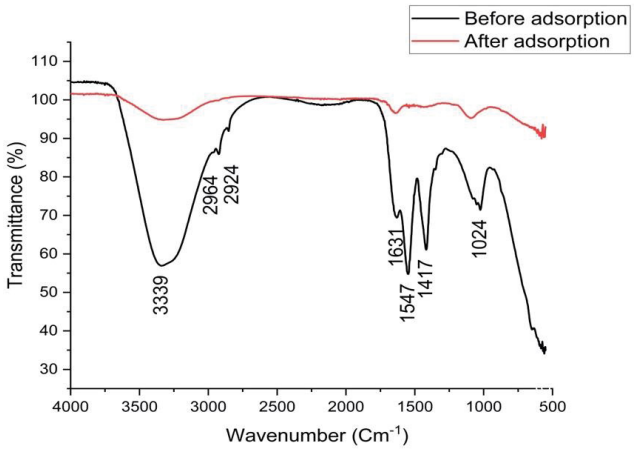

Fig. 8. FTIR spectra of HA acid solution before and after adsorption on BC-MOP.

capacities. Therefore the Langmuir isotherm indicated that all adsorbents had homogeneous surfaces made up of monolayers [20].

3.6. HA acid characterization by FTIR spectra

The FTIR spectra of HA samples before and after adsorption BC-MOP are shown in Fig. 8. The absorption peak at 3,339 cm^{-1} was significantly reduced, and the two absorption peaks at 2,964 cm^{-1} and 2924 cm^{-1} disappeared after adsorption; this indicated that the functional groups of BC-MOP reacted strongly with O–H on HA molecules, leading to the gradual disintegration of this organic matter. The band's intensity at 1,631 cm^{-1} decreased significantly, indicating that the content with internal conjugated double bonds (C=C, C=O) decreased. The peaks at 1,547 and 1417 cm^{-1} disappeared, indicating that the partially saturated hydrocarbon group reacted with functional groups in the BC-MOP surface to form relatively low molecular weight organic compounds. The stretching vibration peak at around 1,024 cm^{-1} shifted to a high value of 1,100 cm^{-1} after adsorption, indicating that BC-MOP reacted strongly with HA.

3.7. HA acid characterization by UV absorption

In the range of wavelengths (200–300 nm), the absorbance fluctuations are illustrated in Fig. 9. With BC-MOP

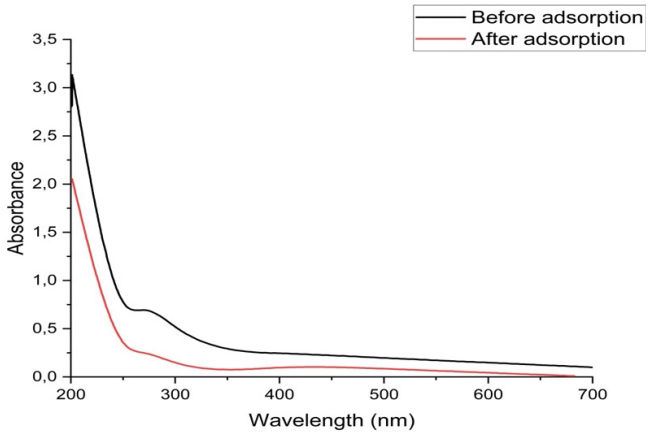

Fig. 9. UV-visible spectra of HA solution before and after adsorption on BC-MOP.

adsorption, the absorbance dropped in this UV range, raising the potential of measuring the organics. Strong absorbance near the UV is caused by particular binding configurations in organic molecules, which is a sign of conjugated systems like those seen in aromatic compounds.

4. Conclusions

In this work, biochar derived from *Moringa* husks was modified by *Moringa* protein to enhance the adsorption performance of humic acid. The sorption process was followed through operating parameters such as pH, contact time, and adsorbent dosage. The pH solution played a crucial role in the adsorption of humic acid on biochar and biochar- *Moringa* protein, which decreased significantly with an increase in solution pH. High adsorption capacity was obtained by Biochar-*Moringa* protein compared to biochar. The kinetics model showed that the pseudo-second-order was a better fit for the experimental data of humic acid adsorption than the pseudo-first-order. The Langmuir model provided a better description of the equilibrium data for the biochar and the biochar-*Moringa* protein. This study revealed that biochar-*Moringa* protein is suitable for use as an adsorbent for humic acid removal from aqueous solution.

Symbols

q_{ad}	—	Amount of HA adsorbent, mg/g
C_0	—	Initial concentration of HA, mg/L
C_e	—	Equilibrium concentration, mg/L
V	—	Volume, L
m	—	Mass of adsorbent, g
q_t	—	Quantity of adsorbate at any given time, t
q_e	—	Amount of adsorbate at equilibrium time, mg g^{-1}
k_1	—	Pseudo-first-order equilibrium rate constant, min^{-1}
k_2	—	Pseudo-second-order equilibrium rate constant, g mg^{-1} min^{-1}
q_m	—	Maximum adsorption capacity, mg g^{-1}

k_L	—	Langmuir constant, L mg^{-1}
K_F	—	Freundlich affinity coefficient, (mg/g)(L/mg)$^{1/n}$
n	—	Measure of adsorption linearity
PZC	—	Point of zero charge

Acknowledgements

The authors would like to thank to the Faculty of sciences and Technology University of ADRAR, Algeria for the XRD analysis.

References

[1] A. Imyim, E. Prapalimrungsi, Humic acids removal from water by aminopropylfunctionalized rice husk ash, J. Hazard. Mater., 184 (2010) 775–781.
[2] Q. Tao, Z. Xu, J. Wang, F. Liu, H. Wan, S. Zheng, Adsorption of humic acid to aminopropyl functionalized SBA-15, Microporous Mesoporous Mater., 131 (2010) 177–185.
[3] C. Li, Y. Dong, D. Wu, L. Peng, H. Kong, Surfactant modified zeolite as adsorbent for removal of humic acid from water, Appl. Clay Sci., 52 (2011) 353–357.
[4] K.L. Jarvis, P. Majewski, Plasma polymerized allylamine coated quartz particles for humic acid removal, J. Colloid Interface Sci., 380 (2012) 150–158.
[5] J.H. Wang, X. Han, H. Ma, Y. Ji, L. Bi, Adsorptive removal of humic acidfrom aqueous solution on polyaniline/attapulgite composite, Chem. Eng. J., 173 (2011) 171–177.
[6] M. Ahmad, A.U. Rajapaksha, J.E. Lim, M. Zhang, N. Bolan, D. Mohan, M. Vithanage, S.S. Lee, Y.S. Ok, Biochar as a sorbent for contaminant management in soil and water: a review, Chemosphere, 99 (2014) 19–33.
[7] A.U. Rajapaksha, S.S. Chen, D.C. Tsang, M. Zhang, M. Vithanage, S. Mandal, B. Gao, N.S. Bolan, Y.S. Ok, Engineered/designer biochar for contaminant removal/immobilization from soil and water: potential and implication of biochar modification, Chemosphere, 148 (2016) 276–291.
[8] J.S. Cha, S.H. Park, S.C. Jung, C. Ryu, J.K. Jeon, M.C. Shin, Y.K. Park, Production and utilization of biochar: a review, J. Ind. Eng. Chem., 40 (2016) 1–15.
[9] N. Cheng, B. Wang, P. Wu, X. Lee, Y. Xing, M. Chen, B. Gao, Adsorption of emerging contaminants from water and wastewater by modified biochar: a review, Environ. Pollut., 273 (2021) 116448.
[10] A. Ndabigengesere, K.S. Narasiah, B.G. Talbot, Active agents and mechanism of coagulation of turbid waters using *Moringa oleifera*, Water Res., 29 (1995) 703–710.
[11] C.Y. Yin, Emerging usage of plant-based coagulants for water and wastewater treatment, Process Biochem., 45 (2010) 1437–1444.
[12] A. Belbali, A. Benghalem, K. Gouttal, S. Taleb, Coagulation of turbid wastewater with an active component extracted from *Moringa oleifera* seeds, Int. J. Environ. Anal. Chem., (2021) 1–17.
[13] Y.S. Ho, G. McKay, The sorption of lead(II) on peat, Water Res., 33 (1999) 578–584.
[14] M.C. Qhubu, L.G. Mgidlana, L.M. Madikizela, V.E. Pakade, Preparation, characterization and application of activated clay biochar composite for removal of Cr(VI) in water: Isotherms, kinetics and thermodynamics, Mater. Chem. Phys., 260 (2021) 124165.
[15] X. Dong, L.Q. Ma, Y. Li, Characteristics and mechanisms of hexavalent chromium removal by biochar from sugar beet tailing, J. Hazard. Mater., 190 (2011) 909–915.
[16] S. Keerthanan, C. Gunawardane, T. Somasundaram, T. Jayampathi, C. Jayasinghe, M. Vithanage, Immobilization and retention of caffeine in soil amended with *Ulva reticulata* biochar, J. Environ. Manage., 281 (2021) 111852.
[17] A. Sarkar, A. Ranjan, B. Paul, Synthesis, characterization and application of surface-modified biochar synthesized from rice husk, an agro-industrial waste for the removal of hexavalent chromium from drinking water at near-neutral pH, Clean Technol. Environ. Policy, 21 (2019) 447–462.
[18] W. Tian, Y. Wang, J. Hao, T. Guo, X. Wang, X. Xiang, Q. Guo, Amine-modified biochar for the efficient adsorption of carbon dioxide in flue gas, Atmosphere, 13 (2022) 579.
[19] Z. Labaali, S. Kholtei, J. Naja, Co^{2+} removal from wastewater using apatite prepared through phosphate waste rock valorisation: equilibrium, kinetic and thermodynamics stadies, Sci. Afr., 8 (2020) e00350.
[20] C. Tsamo, M. Assabe, J. Argue, S.O. Ihimbru, Discoloration of methylene blue and slaughter house wastewater using maize cob biochar produced using a constructed burning chamber: a comparative study, Sci. Afr., 3 (2019) e00078.